

# 000 001 002 003 004 005 006 007 TACKLING THE ABSTRACTION AND REASONING COR- 008 PUS WITH VISION TRANSFORMERS: THE IMPORTANCE 009 OF 2D REPRESENTATION, POSITIONS, AND OBJECTS 010 011

012 **Anonymous authors**  
 013 Paper under double-blind review  
 014  
 015  
 016  
 017  
 018  
 019  
 020  
 021  
 022  
 023  
 024  
 025  
 026  
 027  
 028  
 029  
 030  
 031  
 032

## ABSTRACT

033  
 034 The Abstraction and Reasoning Corpus (ARC) is a popular benchmark focused  
 035 on *visual reasoning* in the evaluation of Artificial Intelligence systems. In its orig-  
 036 inal framing, an ARC task requires solving a program synthesis problem over  
 037 small 2D images using a few input-output training pairs. In this work, we adopt  
 038 the recently popular *data-driven* approach to the ARC and ask whether a Vision  
 039 Transformer (ViT) can learn the implicit mapping, from input image to output  
 040 image, that underlies the task. We show that a ViT—otherwise a state-of-the-art  
 041 model for images—fails dramatically on most ARC tasks even when trained on  
 042 one million examples per task. This points to an inherent representational defi-  
 043 ciency of the ViT architecture that makes it incapable of uncovering the simple  
 044 structured mappings underlying the ARC tasks. Building on these insights, we  
 045 propose ViTARC, a ViT-style architecture that unlocks some of the visual reason-  
 046 ing capabilities required by the ARC. Specifically, we use a pixel-level input rep-  
 047 resentation, design a spatially-aware tokenization scheme, and introduce a novel  
 048 object-based positional encoding that leverages automatic segmentation, among  
 049 other enhancements. Our task-specific ViTARC models achieve a test solve rate  
 050 close to 100% on more than half of the 400 public ARC tasks strictly through su-  
 051 pervised learning from input-output grids. This calls attention to the importance  
 052 of imbuing the powerful (Vision) Transformer with the correct inductive biases for  
 053 abstract visual reasoning that are critical even when the training data is plentiful  
 054 and the mapping is noise-free. Hence, ViTARC provides a strong foundation for  
 055 future research in visual reasoning using transformer-based architectures.

## 1 INTRODUCTION

056  
 057 Developing systems that are capable of performing abstract reasoning has been a long-standing  
 058 challenge in Artificial Intelligence (AI). Abstract Visual Reasoning (AVR) tasks require AI models  
 059 to discern patterns and underlying rules within visual content, offering a rigorous test for eval-  
 060 uating AI systems. Unlike other visual reasoning benchmarks such as Visual Question Answering  
 061 (VQA) (Antol et al., 2015) and Visual Commonsense Reasoning (VCR) (Kahou et al., 2018) that  
 062 rely on natural language inputs or knowledge of real-world physical properties, AVR tasks do not  
 063 include any text or background knowledge. Instead, they focus purely on visual abstraction and  
 064 pattern recognition (Małkiński & Mańdziuk, 2023). One prominent example of AVR is the Abstrac-  
 065 tion and Reasoning Corpus (ARC) (Chollet, 2019), which is designed to evaluate an AI’s capacity  
 066 for generalization in abstract reasoning. Each ARC task involves transforming input grids into out-  
 067 put grids by identifying a hidden mapping often requiring significant reasoning beyond mere pattern  
 068 matching (cf. Figure 2). While the ARC’s original setting is one of few-shot learning, there has been  
 069 recent interest in studying the ARC in a data-rich setting where task-specific input-output samples  
 070 can be generated (Hodel, 2024), allowing for the evaluation of deep learning-based solutions.

071  
 072 In this paper, we explore the potential of vision transformers to solve ARC tasks using supervised  
 073 learning. We assess how well transformers can learn complex mappings for a single task when pro-  
 074 vided with sufficient training data. Our exploration highlights fundamental representational limita-  
 075 tions of vision transformers on the ARC, leading to three high-level findings that we believe provide  
 076 a strong foundation for future research in visual reasoning using transformer-based architectures:

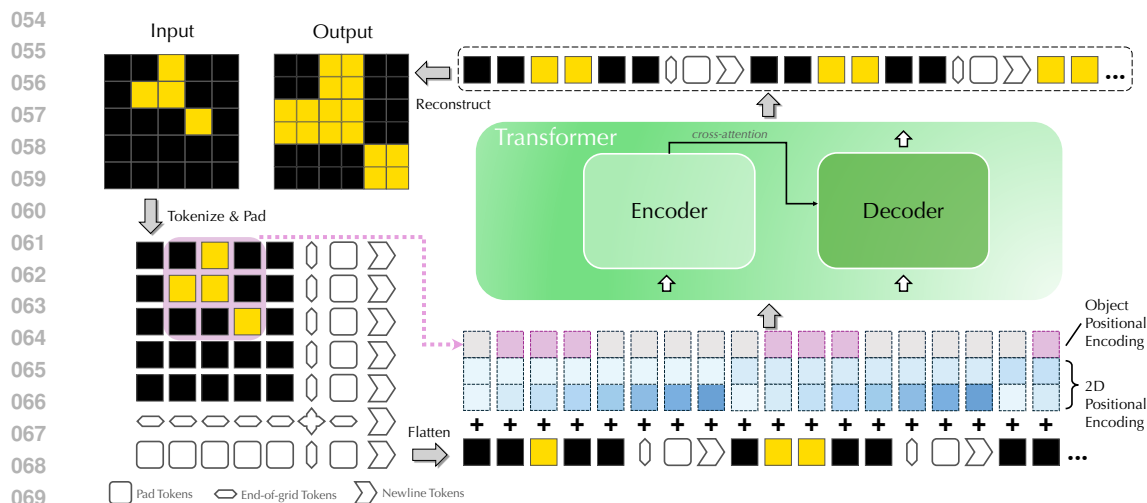


Figure 1: **Overview of our ViTARC framework contribution.** An ARC input image is first tokenized into pixels and padded with visual tokens including end-of-grid tokens that mark the end of the image grid, newline tokens that indicate the end of one row, and pad tokens which are used to pad the image into a fixed maximum size (not drawn in full to maintain clarity). 2D Positional Encodings and Object Positional Encodings are then added to each token before being passed into the transformer. The output tokens are reconstructed into a valid two-dimensional grid.

1. **A vanilla Vision Transformer (ViT) fails on the ARC:** Despite the ARC grids’ relatively simple structure compared to the much larger, noisier natural images they are typically evaluated on, a vanilla ViT performs extremely poorly on 90% of the tasks with an overall test accuracy of 18% (cf. Figure 3, Section 3). This is despite using a training set of one million examples per task. Following a failure analysis, we hypothesize that the vanilla ViT fails because it cannot accurately model spatial relationships between the objects in an ARC grid and the grid boundaries.

2. **A 2D visual representation significantly boosts ViT reasoning performance:** Using a 2D representation strategy based on *visual tokens* to represent the ARC input-output pairs, ViTARC solves 66% of all test instances – a marked improvement (cf. Section 4). About 10% of the tasks remain poorly solved. After further failure analysis on these tasks, we discover that certain complex visual structures are difficult for ViTARC. We hypothesize this is due to limitations of the transformer architecture itself in that it is designed to prioritize token embeddings over positional encodings that can make it challenging to capture intricate spatial relationships.

3. **Positional Information further enhances ViT reasoning abilities:** We improved ViTARC’s spatial awareness by learning to combine absolute, relative, and *object* positional information (cf. Section 5), resulting in substantial performance boosts, with some ARC tasks progressing from unsolved to fully solved (Figure 3). The final test accuracy is 75%, with more than half of the tasks being solved to an accuracy of 95% or more.

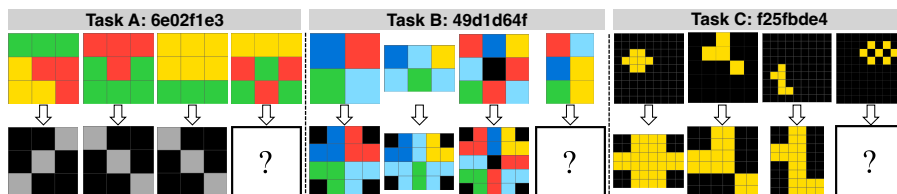


Figure 2: **Three example ARC tasks.** For each task, the first columns contain example input-output pairs from the “training” instances, and the last column contains the “test” instance. The goal is to use the training instances to solve the test instance. The Vanilla ViT setup (Section 3) was only able to solve Task A<sup>1</sup>. Our VitARC-VT (Section 4) was able to solve Task A and B but still failed at Task C. Our final model ViTARC (Section 5) achieves near 100% accuracy on all three tasks.

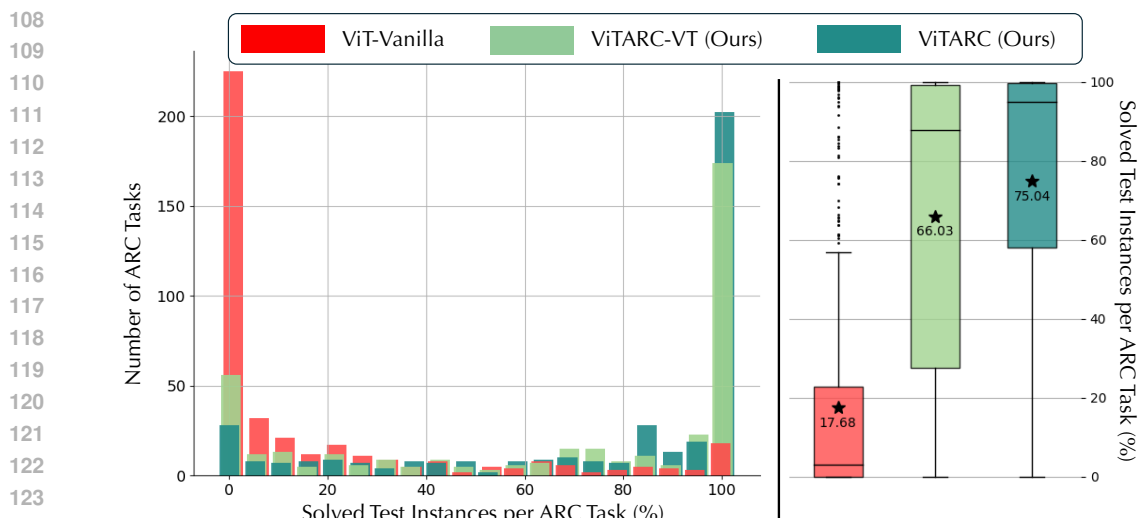


Figure 3: **Model performances on 400 ARC tasks.** Three models are shown: ViT-Vanilla (red) represents the vanilla vision transformer setup (cf. Section 3); ViTARC-VT (light green) and ViTARC (dark green) represent the variants of our framework introduced in Sections 4 and 5, respectively. (Left) Distribution of Solve Rates: The horizontal axis shows the solve rate (percentage of test instances that are solved correctly) on 1000 test instances per task. The vertical axis displays the number of tasks at each solve rate level. (Right) Distribution Statistics: The stars and corresponding values are the overall solve rates across all test instances from all tasks. ViTARC-VT and ViTARC show significant improvement in performance over the vanilla ViT.

## 2 RELATED WORK

**Abstract Visual Reasoning (AVR)** is an emerging field that seeks to measure machine “intelligence” (Małkiński & Mańdziuk, 2023). Unlike many popular studies that focus on visual reasoning with multi-modal input (Antol et al., 2015; Johnson et al., 2017; Zellers et al., 2019; Bakhtin et al., 2019; Li et al., 2024), AVR focuses on reasoning tasks where the inputs are strictly images. The goal of AVR tasks is to discover abstract visual concepts and apply them to new settings. While the ARC is a generation task using abstract rules, other AVR tasks include classification tasks with explicit rules, such as the Raven’s Progressive Matrices (Raven, 2003) and Odd-One-Out (Gardner & Richards, 2006). We refer the readers to Małkiński & Mańdziuk (2023) for a more detailed introduction to AVR.

**Vision Transformers & Positional Encoding.** A Transformer architecture is based on the attention mechanism (Vaswani et al., 2017). Following successes in natural language processing (Brown et al., 2020; Achiam et al., 2023; Devlin et al., 2019), recent studies have extended the Transformer to the vision domain (Han et al., 2023). State-of-the-art approaches involve dividing the image into rectangular “patches”(Dosovitskiy et al., 2021), where various techniques such as dynamic patch sizes allow for more effective capture of local information (Havtorn et al., 2023; Zhou & Zhu, 2023). Vision Transformers have been successfully used to perform various image-to-image generation tasks such as inpainting (Li et al., 2022), image restoration (Liang et al., 2021), colorization (Kumar et al.), and denoising (Wang et al., 2022).

Due to the set-based (permutation-invariant) nature of attention, Positional Encodings are used to inject positional information in a Transformer (Vaswani et al., 2017). State-of-the-art Positional Encodings include Absolute Positional Encodings (APEs) where unique encodings are added to the inputs directly (Devlin et al., 2019), Additive Relative Positional Encodings (RPEs) (Shaw et al.,

<sup>1</sup>Task A follows a rule based on color count: if the input grid has two distinct colors, the output contains a grey diagonal from the top-left to the bottom-right. Conversely, if the input grid has three colors, the grey diagonal is from the top-right to the bottom-left.

162 2018; Raffel et al., 2020; Li et al.) that measure the relative positions between tokens by modifying  
 163 the attention logits, and various hybrid methods (Su et al., 2024; Zhou et al., 2024). Vision Trans-  
 164 former research has adapted these concepts, implementing both APEs (Dosovitskiy et al., 2021) and  
 165 RPEs (Wu et al., 2021) to incorporate positional information about the image patches.  
 166

167 **Solvers for the ARC.** Since the introduction of the ARC (Chollet, 2019), the development of  
 168 solvers has been an active research area. The earliest successful approaches consisted of an ex-  
 169 pressive Domain Specific Language (DSL) and a program synthesis algorithm that searched for a  
 170 valid solution program expressed in the DSL. These include DAG-based search (Wind, 2020), graph-  
 171 based constraint-guided search (Xu et al., 2023), grammatical evolution (Fischer et al., 2020), library  
 172 learning (Alford et al., 2021), compositional imagination (Assouel et al., 2022), inductive logic pro-  
 173 gramming (Hocquette & Cropper, 2024), decision transformers (Park et al., 2023), generalized plan-  
 174 ning (Lei et al., 2024), reinforcement learning (Lee et al., 2024), and several others (Ainooson et al.,  
 175 2023; Ferré, 2021). These models achieved up to 30% on the private ARC test set (Chollet et al.,  
 176 2020; Lab42, 2023).

177 Recently, Transformer-based Large Language Models (LLMs) were shown to exhibit an apparent  
 178 ability to perform “reasoning” (Wei et al., 2022) spurring interest in using LLMs as part of an ARC  
 179 solver. Such methods were prompted to perform program synthesis on a DSL (Min Tan & Motani,  
 180 2024; Barke et al., 2024) as well as general-purpose languages such as Python (Butt et al., 2024;  
 181 Wang et al., 2024), with the best-performing model achieving 42% on the public ARC evaluation  
 182 set (Greenblatt, 2024). LLMs were also explored as standalone solvers, where they were asked  
 183 to produce the output grids directly instead of outputting a program. Although pre-trained LLMs  
 184 proved ineffective when generating the output grid pixels directly (Camposampiero et al., 2023;  
 185 Mirchandani et al., 2023; Moskvichev et al., 2023), its performance was shown to be improved by  
 186 object representation (Xu et al., 2024). The vision variant of a state-of-the-art LLM, GPT-4V was  
 187 shown to be ineffective (Mitchell et al., 2023; Xu et al., 2024).

188 The current state-of-the-art solver has achieved 46% on the private test set at the time of writing (ar-  
 189 cprize, 2024) but is not publicly available or described in detail. We do know that it is a pre-trained  
 190 LLM that is fine-tuned on millions of synthetic ARC tasks generated using the RE-ARC gener-  
 191 ator (Hodel, 2024) and combined with test-time fine-tuning (Cole & Osman, 2023). Despite the  
 192 visual nature of ARC tasks, Transformer-based LLM approaches convert the images into strings,  
 193 which does not fully capture all relevant structural information (Xu et al., 2024).

### 194 3 VANILLA VISION TRANSFORMER FOR THE ARC: AN INITIAL APPROACH 195

196 We first implement a vanilla Vision Transformer architecture as detailed in Dosovitskiy et al. (2021)  
 197 and Touvron et al. (2021) as a solver for the ARC. Consider an input image  $I$  divided into  $P \times P$   
 198 non-overlapping patches. Each patch  $p_i$  is flattened in raster order and indexed by  $i$  before being  
 199 projected into a  $d$ -dimensional embedding space. Let  $h_i^0$  denote the initial input to the Transformer  
 200 for patch  $p_i$ . For the  $n$ -th Transformer layer,  $n \in \{1, \dots, N\}$ , and for a single attention head, the  
 201 following operations are performed:

$$h_i^0 = \mathbf{E}_{p_i} + \mathbf{E}_{\text{pos}_i} \quad (1)$$

$$\hat{h}_i^n = \text{LayerNorm}(h_i^{n-1}) \quad (2)$$

$$q_i^n, k_i^n, v_i^n = \hat{h}_i^n \mathbf{W}_q^n, \quad \hat{h}_i^n \mathbf{W}_k^n, \quad \hat{h}_i^n \mathbf{W}_v^n \quad (3)$$

$$A_{i,j}^n = \frac{q_i^n \cdot k_j^n}{\sqrt{d}} \quad (4)$$

$$o_i^n = \sum_j \text{Softmax}(A_{i,j}^n) v_j^n + h_i^{n-1} \quad (5)$$

$$f_i^n = \text{FeedForward}(\text{LayerNorm}(o_i^n)) + o_i^n \quad (6)$$

$$h_i^n = \text{LayerNorm}(f_i^n) \quad (7)$$

214 Here,  $\mathbf{E}_{p_i}$  is the embedding of patch  $p_i$  and  $\mathbf{E}_{\text{pos}_i}$  is the positional encoding. Following the stan-  
 215 dard ViT implementation of Dosovitskiy et al. (2021), the Absolute Positional Encoding (APE) is

216 calculated as a learnable 1D encoding:  
 217

$$\mathbf{E}_{\text{pos}_i} = \mathbf{W}_i, \quad \mathbf{E}_{\text{pos}_i} \in \mathbb{R}^d, \quad \mathbf{W} \in \mathbb{R}^{L \times d}$$

220 where  $\mathbf{W}$  is a learned matrix assigning a  $d$ -dimensional vector to each of the possible  $L$  positions;  
 221  $L$  is the maximum input length.

222 As seen in Figure 2, ARC tasks are *generative* and require mapping an input image to an output  
 223 image. Because image dimensions may vary across instances of the same task and even between  
 224 the input and output grids of the same instance, any model that generates candidate solutions to an  
 225 ARC input must be able to “reason” at the pixel level. We adapt the ViT architecture to this setting  
 226 by making the following key modifications:

- 228 – We introduce a decoder with cross-attention using the same positional encoding and attention  
 229 mechanisms of the encoder. After the final decoder layer  $N$ , the output embedding  $h_i^N$  of  
 230 patch  $i$  is projected linearly and a softmax function is applied to predict pixel-wise values  $\hat{y}_i$   
 231 as  $\hat{y}_i = \text{Softmax}(\text{Linear}(h_i^N))$ . The cross-entropy loss is computed as the sum over pixels,  
 232  $-\sum_i y_i \log(\hat{y}_i)$ .
- 233 – To achieve the required pixel-level precision for the ARC task, we employ a patch size of  $1 \times 1$ ,  
 234 effectively treating each pixel as an independent input token.
- 235 – To handle variable-sized grids, the flattened list of tokens is padded to a fixed maximum length.  
 236 This configuration enables the model to process and generate ARC task outputs pixel-by-pixel.

### 238 3.1 EXPERIMENTS

240 **Data.** To evaluate ViT’s reasoning capabilities comprehensively, we treat each of the 400 public  
 241 training ARC tasks as an individual AVR problem. We generate a dataset of 1 million input-output  
 242 pairs per task using the RE-ARC generator (Hodel, 2024) and train all of our models (the vanilla  
 243 ViT and ViTARC models) in a supervised manner from scratch.

245 **Hyperparameters and training protocol.** The ViT baseline consists of three layers with eight  
 246 attention heads and a hidden dimension of 128. We trained the model on various single-core GPU  
 247 nodes, including P100, V100, and T4, using a batch size of 8 for one epoch. We chose to train for one  
 248 epoch because most models showed signs of convergence within the epoch. Due to computational  
 249 resource limitations, we evaluated our major milestone models on the full set of 400 tasks. However,  
 250 for the ablation studies hereafter, we used a randomly sampled subset of 100 tasks. For more details  
 251 on the training process, please refer to Appendix B. Our code is available in the supplementary  
 252 materials and will be open-sourced upon publication.

253 **Evaluation metric.** We evaluate the model primarily on the percentage of solved instances, using  
 254 a strict criterion: an instance is considered solved only if all generated pixels, including padding  
 255 and border tokens, exactly match the ground truth. This approach is stricter than the original ARC  
 256 metric which permits up to three candidate solutions.

258 **Results.** Figure 3 shows that the vanilla ViT performs poorly: a significant percentage of tasks  
 259 have a near 0% solve rate despite the million training examples per task. This points to fundamental  
 260 limitations of the ViT architecture that inhibit abstract visual reasoning. In the following sections,  
 261 we analyze failure cases and investigate methods for enhancing the visual reasoning ability of ViT.

## 263 4 VISUAL TOKENS: A BETTER REPRESENTATION FOR ViT

266 The basic version of our ViTARC framework builds on the vanilla ViT but includes three simple yet  
 267 highly effective changes to the representation of the ARC grids. We refer to these changes as *visual*  
 268 *tokens* to emphasize a departure from the language-based tokenization perspective in the particular  
 269 setting of the ARC.

270  
 271   **2D padding.** We observed that a  
 272 large portion of the incorrect outputs  
 273 from the vanilla ViT had incorrect  
 274 grid sizes, a flagrant failure mode;  
 275 An example is visualized in Figure 4  
 276 (ViT-Vanilla). We hypothesize that  
 277 this is due to the vanilla ViT imple-  
 278 menting padding in a “1D” manner,  
 279 where  $\langle \text{pad} \rangle$  tokens are applied to  
 280 the sequence after flattening, thus los-  
 281 ing the two-dimensional context. To  
 282 address this issue, we implemented  
 283 2D padding, where  $\langle \text{pad} \rangle$  tokens  
 284 are applied to the image *first* before  
 285 being flattened in raster order into a  
 286 sequence for transformer processing  
 287 (see Figure 1).

288   However, this design introduces a  
 289 new drawback: the model must now  
 290 predict  $\langle \text{pad} \rangle$  tokens as part of the  
 291 output grid. In initial experiments, we  
 292 observed that the model tends to ignore these  $\langle \text{pad} \rangle$  tokens  
 293 (that do not receive attention), erroneously predicting over the entire  $h_{\max} \times w_{\max}$  grid rather than  
 294 focusing on the valid input region. An example of this issue is shown in Figure 8 of Appendix A. To  
 295 address this, we define  $\langle 2d\_pad \rangle$  tokens and enable attention to these tokens, allowing the model  
 296 to properly account for the padded regions as well as the valid output region.

297   **Border tokens for spatial awareness.** The implementation of 2D padding did not completely al-  
 298 leviate the previously observed failure cases. We further observed that for some tasks, when the  
 299 output is cropped to the true grid dimensions, the predictions within the valid region are correct,  
 300 underscoring the importance of proper boundary handling. We show an example in Figure 8 of Ap-  
 301 pendix A. Inspired by the use of end-of-sequence (EOS) tokens like  $\langle /s \rangle$  in Natural Language  
 302 Processing (NLP), we introduce *border tokens* to explicitly define the grid boundaries (cf. Figure 1):

- 303   – **Newline tokens** ( $\langle 2d\_nl \rangle$ ) mark row transitions in the  $h_{\max} \times w_{\max}$  grid.
- 304   – **End-of-grid tokens** ( $\langle 2d\_endxgrid \rangle$ ,  $\langle 2d\_endygrid \rangle$ , and  $\langle 2d\_endxygrid \rangle$ ) delin-  
 305    einate the true  $h \times w$  grid boundaries.

306   The introduction of border tokens enables the model to more effectively distinguish the task grid  
 307 from the padding. Without these tokens, the model would need to count tokens to determine bound-  
 308 aries, which becomes unreliable—especially in ARC tasks with dynamically defined output grid  
 309 sizes (e.g., task C in Figure 2). Furthermore, as we see in ViT-Vanilla failure cases (Figure 4), it  
 310 is ambiguous to recover the 2D positions from a 1D sequence of predicted tokens alone. Border  
 311 tokens also provide a fixed 2D template to fill in, which implicitly helps reconstruct the correct 2D  
 312 positions and makes it easier to debug the related grid logic.

313   **2D Absolute Positional Encoding.** With the introduction of 2D padding and border tokens, our  
 314 setup now operates on fixed-size, two-dimensional input-output pairs that are aligned with a univer-  
 315 sal  $(x, y)$  coordinate system. This allows us to adopt existing positional encoding (PE) strategies  
 316 from the literature (see Section 2). After empirical analysis, we implement a (non-learned) 2D  
 317 sinusoidal APE for ViTARC, which is defined as follows:

$$\text{Sinusoid}(p) = \left[ \begin{array}{c} \sin\left(\frac{p}{10000^{2k/d}}\right) \\ \cos\left(\frac{p}{10000^{2k/d}}\right) \end{array} \right], \quad k = 0, \dots, d/2, \quad (8)$$

$$\mathbf{E}_{\text{pos}_{(x,y)}} = \text{concat}(\text{sinusoid}(x), \text{sinusoid}(y)), \quad (9)$$

318   where  $p$  represents either the  $x$  or  $y$  coordinate,  $k$  is the index of the positional encoding dimension,  
 319 and  $d$  is the total embedding dimension.

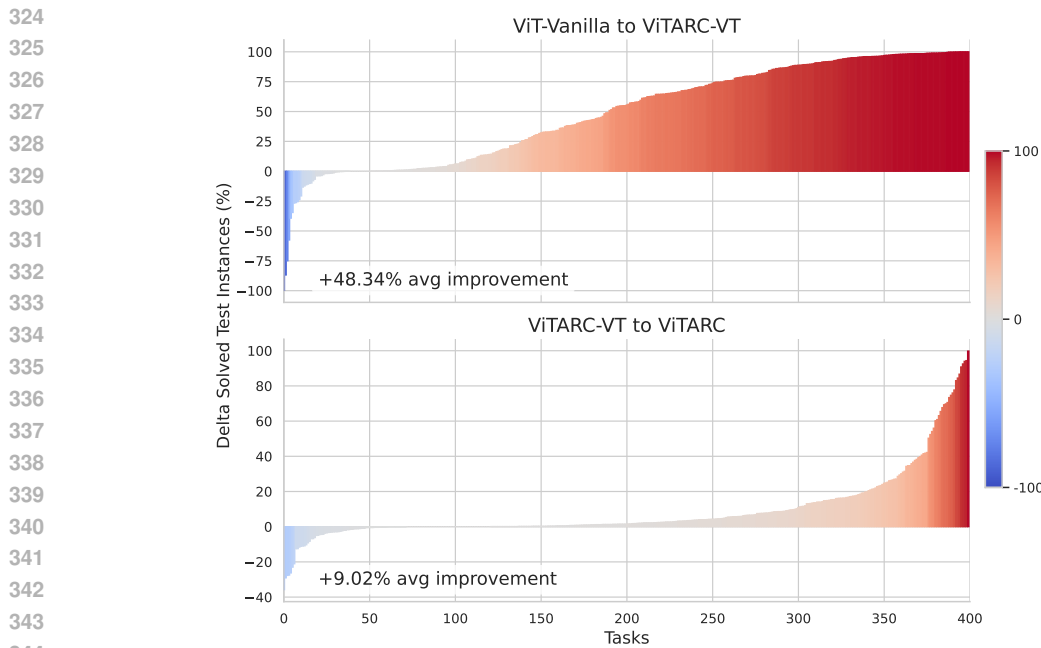


Figure 5: **Improvement in percentage of solved test instances per task.** (a) From ViT-Vanilla to ViTARC-VT: We observe that over 85% of tasks benefit from the introduction of 2D Visual Tokens, showing consistent gains compared to the vanilla ViT. (b) From ViTARC-VT to ViTARC: We observe that more than half of all tasks show further improvement. Improvement from ViT-Vanilla to ViTARC is shown in Figure 9 in Appendix C.1 where a 57.36% average improvement is observed.

#### 4.1 RESULTS

Figure 3 shows substantial improvements in test accuracy due to the 2D visual tokens just described. Figure 5(a) illustrates the improvement in the percentage of solved instances for each task. We observe an average performance boost of 48.34% compared to the baseline ViT across the 400 tasks. This model, referred to as ViTARC-VT, demonstrates that the new representation with 2D visual tokens significantly enhances the model’s ability to handle AVR tasks.

A key driver of this improvement is the use of 2D padding, which creates a fixed schema for 2D positions. This ensures consistent spatial alignment and effectively addresses the challenge of applying 2DAPE to variable-sized grids, where unknown output positions during inference complicate accurate mapping.

To quantify the contribution of border tokens, we performed an ablation study. As seen in Figure 7, the absence of border tokens leads to a 4.59% decrease in accuracy, emphasizing their importance in helping the model delineate task grid boundaries and maintain spatial consistency in the input representation. For more detailed numerical results, refer to Table 6 in Appendix C.2.

#### 4.2 ANALYSIS

While ViTARC-VT delivers strong results—approximately 40% of ARC tasks achieved over 90% solved test instances—there remain certain tasks where the model struggles. Specifically, around 10% of ARC tasks have less than 5% of test instances solved, even after training on a large dataset containing one million examples per task. Closer examination reveals that tasks involving complex visual structures, such as concave shapes, holes, or subgrids, are consistently problematic. These challenges highlight certain architectural limitations, particularly the model’s difficulty in segmenting multi-colored objects, where positional information should ideally play a more dominant role.

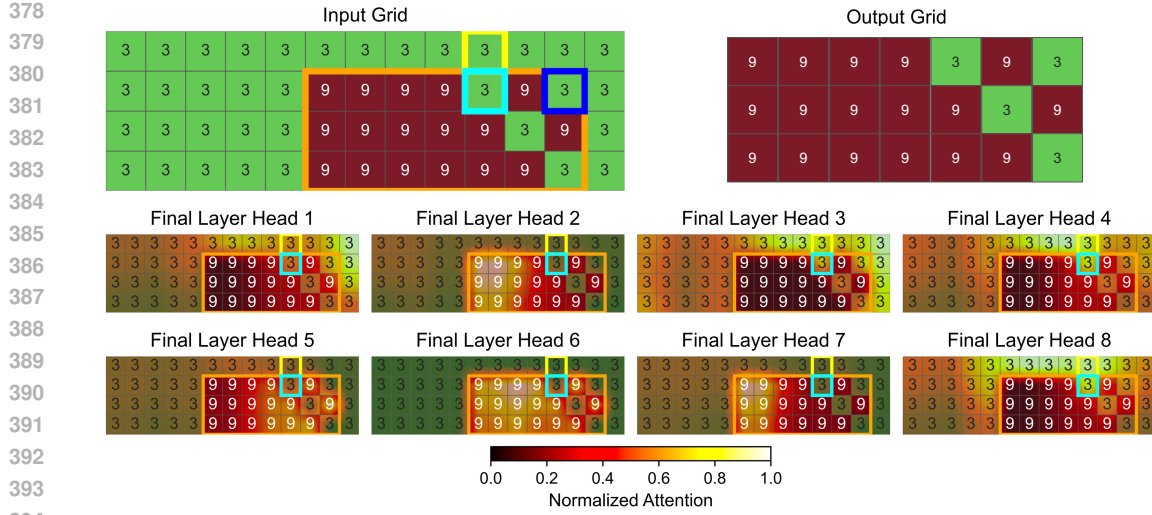


Figure 6: **ViTARC-VT failure analysis for ARC task (#1cf80156).** Cross-attention heatmap across all attention heads in the final layer at the step predicting the color-3 pixel within the dark blue box. The task requires finding the maximum rectangular subgrid in the input. The attention, visualized in a thermal heatmap, shows that none of the heads successfully distinguish the subgrid (orange bounding box) from its surroundings that motivates the PEMixer and OPE, nor do they differentiate the color-3 pixel inside the cyan box (within the subgrid) from the pixel in the yellow box (outside the subgrid) that motivates the 2D-RPE directional bias.

To better understand this behavior, we refer back to Equation (1):  $h_i^0 = \mathbf{E}_{p_i} + \mathbf{E}_{pos_i}$ . In this setup, the absolute positional encoding,  $\mathbf{E}_{pos_i}$ , is directly added to the input embedding,  $\mathbf{E}_{p_i}$ , so that it adjusts the token’s representation without overwhelming its semantic content. This works effectively in NLP tasks, where the semantic meaning of tokens generally takes precedence over their position. However, in vision tasks, especially those requiring detailed visual reasoning, spatial relationships often carry as much importance as, if not more than, the content of the tokens. For tasks in the ARC that involve complex multi-colored objects, such as subgrids, accurately encoding positional information becomes crucial. Figure 6 illustrates a specific case where the model fails to group pixels within a multi-colored subgrid correctly. The cross-attention map reveals that the model overly relies on color similarity, resulting in confusion between similarly colored pixels in different positions. This indicates a lack of sufficient attention to spatial relationships, which is essential for such tasks and guides us to develop further enhancements in the next section.

## 5 RECENTERING POSITIONS & OBJECTS FOR SPATIAL REASONING IN ViT

Our observations on the failure cases of ViTARC-VT lead us to implement further enhancements to tackle tasks with complex visual structures by better encapsulating the positional information of pixels and objects.

**Positional Encoding Mixer (PEmixer).** To better balance the importance of positional information and tokens, we modify Equation (1) by learning weight vectors for the encodings, i.e.,

$$h_i^0 = \boldsymbol{\alpha} \odot \mathbf{E}_{p_i} + \boldsymbol{\beta} \odot \mathbf{E}_{pos_i}, \quad (10)$$

where  $\boldsymbol{\alpha}$  and  $\boldsymbol{\beta}$  are **learnable** vectors of the same dimension as the encoding vectors, and  $\odot$  denotes element-wise multiplication. This effectively allows the model to learn the optimal balance between input tokens and positional encoding.

Furthermore, our implementation of 2D APE as described in Section 4, where  $\mathbf{E}_{pos_{(x,y)}}$  is the concatenation of  $\mathbf{E}_{pos_x}$  and  $\mathbf{E}_{pos_y}$ , allows the vector-based mixing coefficients to focus on specific coordinates, which further improves the model’s reasoning capability over specific pixels.

**432 2D Relative Positional Encoding (2D-RPE).** Motivated by the example in Figure 6, we aim to  
**433** enable the model to distinguish between pixels in different spatial regions, such as the color-3 (green)  
**434** pixel in the cyan box versus the one in the yellow box. In this example, the positional difference  
**435** between the two pixels is just 1 along the  $y$ -coordinate. APE encodes this difference as a small shift;  
**436** while the transformer is theoretically capable of capturing these spatial relationships, in practice  
**437** often requires many training epochs (Hahn, 2020).

**438** To better account for spatial relationships in two-dimensional grids, we adapt the Relative Positional  
**439** Encoding (RPE) approach from ALiBi (Press et al., 2021) and extend it to 2D. ALiBi introduces  
**440** additive positional biases to the attention scores based on the relative positions of tokens. In its  
**441** original 1D form, ALiBi defines the positional bias as the following:

$$\mathbf{A}_{i,j}^n = \frac{\mathbf{q}_i^n \cdot \mathbf{k}_j^n}{\sqrt{d}} + \mathbf{B}_{\mathbf{P}_{i,j}}, \quad \mathbf{B}_{\mathbf{P}_{i,j}} = r \cdot |i - j|, \quad (11)$$

**445** where  $\mathbf{P}_{i,j}$  represents the relative positional offset between tokens  $i$  and  $j$ , and  $r$  is a predefined  
**446** slope that penalizes tokens based on their distance.

**447** Extending to 2D, we introduce distinct slopes for the “left” and “right” directions, efficiently cap-  
**448** turing directional biases along the x and y axes. This design leverages the inherent 2D structure of  
**449** the data while aligning with the sequential raster order of the generation process. Specifically:  
**450**

- 451** – Pixels located above or to the left of the current pixel in 2D space are assigned a bias  $r_{\text{left}}$ .
- 452** – Pixels located below or to the right are assigned a bias  $r_{\text{right}}$ .

**454** Hence, the 2D-RPE bias is computed as:

$$\mathbf{B}_{\mathbf{P}_{i,j}} = \begin{cases} r_{\text{left}} \cdot d((x_i, y_i), (x_j, y_j)), & \text{if } j \leq i, \\ r_{\text{right}} \cdot d((x_i, y_i), (x_j, y_j)), & \text{if } j > i, \end{cases} \quad (12)$$

**458** where  $d((x_i, y_i), (x_j, y_j))$  represents the 2D Manhattan distance between coordinates  $(x_i, y_i)$  and  
**459**  $(x_j, y_j)$ . The slope values  $r_{\text{left}}$  and  $r_{\text{right}}$  are derived following the ALiBi setup, forming a geometric  
**460** sequence of the form  $2^{-8/n}$  for  $n$  heads.  $r_{\text{left}}$  starts at  $1/2^1$ , while  $r_{\text{right}}$  starts at  $1/2^{0.5}$ , both using  
**461** the same ratio.

**462** In this work, we leverage both 2D-RPE and 2D sinusoidal APE within our model. In contrast  
**463** to observations made in Swin (Liu et al., 2021), where a degradation in performance was noted  
**464** when combining RPE with APE, our results demonstrate a marked improvement. The inclusion  
**465** of 2D-RPE allows for more precise modeling of relative spatial relationships, complementing the  
**466** global positional information provided by APE. This synergy proves particularly effective for tasks  
**467** demanding fine-grained spatial reasoning.  
**468**

**469** **Object-based Positional Encoding (OPE).** For tasks involving multi-colored objects, or more  
**470** generally, tasks that require objectness priors (Chollet, 2019), external sources of knowledge about  
**471** object abstractions can be integrated into the model. We inject this information through a novel  
**472** *object-based positional encoding*. We extend the 2D sinusoidal APE defined in Equation (9) by  
**473** introducing the object index  $o$  as an additional component to the pixel coordinates  $(x, y)$ . This  
**474** results in a modified positional encoding:

$$\mathbf{E}_{\text{pos}_{(o,x,y)}} = \text{concat}(\text{sinusoid}(o), \text{sinusoid}(x), \text{sinusoid}(y)). \quad (13)$$

**477** In object detection models, two primary segmentation methods are bounding box segmentation and  
**478** instance segmentation, the latter of which captures precise object boundaries. For simplicity, we  
**479** adopt bounding box segmentation to derive the object index  $o$ , as fine-grained distinctions at the  
**480** instance level can already be addressed by the model’s attention mechanism, as illustrated in Fig-  
**481** ure 6. Figure 1 demonstrates how bounding box information is obtained and incorporated into the  
**482** positional encoding.

**483** This design integrates seamlessly with the PEmixer introduced earlier, as it enables the model to  
**484** dynamically adjust its reliance on the object index  $o$  based on the task’s needs. In scenarios where  
**485** the object index provides valuable abstraction, the model can prioritize it, while in cases where the  
**486** object-based method is less effective, the model can fall back on the  $(x, y)$  positional information.

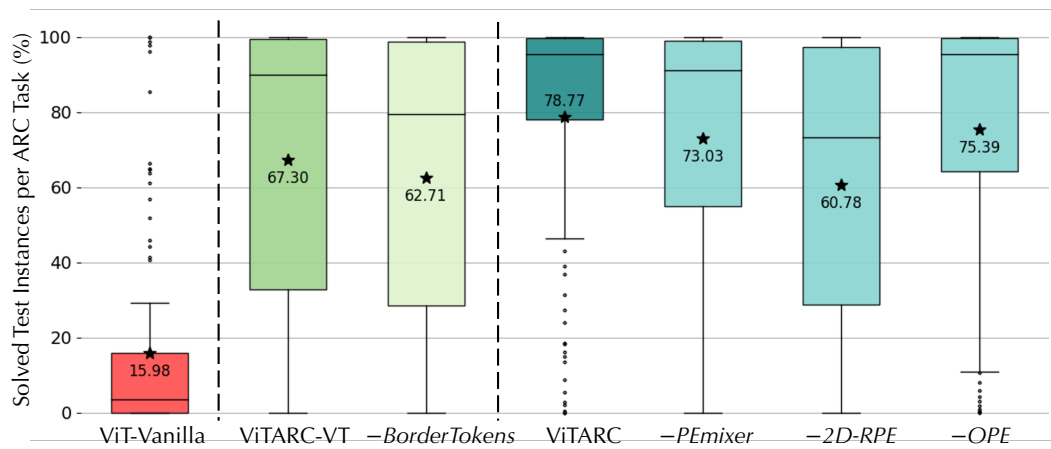


Figure 7: **Distribution statistics of solve rates on 100 random tasks for ablation.** 7 Models are shown: ViT-Vanilla, ViTARC-VT, and ViTARC are the models introduced in Sections 3, 4 and 5 respectively. Ablated components are prefixed as  $-$  and ablate the full model to the left, i.e.,  $-BorderTokens$  is an ablation of this component from ViTARC-VT and each of  $-PEmixer$ ,  $-2D-RPE$ , and  $-OPE$  ablate these respective components from ViTARC.

For our experiments, OpenCV’s contour detection (Bradski, 2000) proved sufficient for generating object indices in the ARC tasks, demonstrating the practical effectiveness of OPE. This novel approach not only addresses challenges related to complex object shapes but also establishes a method for injecting external objectness knowledge into vision models, enhancing their reasoning capabilities.

## 5.1 RESULTS

We arrive at our final model, ViTARC, which contains all the improvements mentioned in Section 4 and Section 5. The final encoding combines all three components: 2DAPE, 2DRPE, and OPE, leveraging their complementary strengths to enhance spatial reasoning. As shown in Figure 3, the model is a significant improvement over both the baseline ViT-Vanilla and ViTARC-VT due to the proposed positional enhancements.

Furthermore, Figure 5(b) highlights the generalization of these improvements across tasks, with an additional 9.02% increase in solved instances compared to ViTARC-VT. ViTARC-VT itself already achieved a significant boost over ViT-Vanilla, culminating in a total improvement of 57.36% over the baseline ViT-Vanilla.

Figure 7 further illustrates the impact of each enhancement on task performance. All three contribute to the overall improvement, with 2D-RPE providing the largest gain, followed by PEmixer and OPE. Notably, without 2D-RPE, the model’s performance drops below that of ViTARC-VT. This occurs because OPE, while effective in specific tasks, is not consistently reliable. In these cases, ViTARC must fall back on the  $(x, y)$  embeddings from 2D-APE, which are less expressive due to their lower dimensionality compared to ViTARC-VT. The inclusion of 2D-RPE recovers these positional signals at the attention level, ensuring robust performance even when object-based cues are insufficient.

For a comprehensive breakdown of the task-level performance and the numerical details of these ablations, please refer to Appendix C.2.

## 6 CONCLUSION

This paper introduced ViTARC, a Vision Transformer architecture designed to address the unique challenges posed by the Abstraction and Reasoning Corpus. A key finding of our work is that positional information plays a critical role in visual reasoning tasks. While often overlooked when adapting transformers from NLP to vision, our results demonstrate that even simple enhancements

540 to positional encoding can significantly improve performance on ARC tasks. Furthermore, we show  
 541 that incorporating object indices as additional positional information via OPEs provides a meaningful  
 542 improvement in handling complex spatial relationships in ARC tasks.

543 Additionally, we introduced 2D padding and border tokens to handle variable-sized images requiring  
 544 high precision in visual reasoning. Given ARC’s pixel-level precision and abstract reasoning  
 545 requirements (e.g., 1x1 pixel tasks in ARC, but potentially  $n \times n$  pixels in more generalized visual  
 546 reasoning), resizing or cropping—commonly used in standard vision tasks—is infeasible. ViTARC  
 547 reveals limitations in current ViT structures under these conditions and suggests necessary adapta-  
 548 tions for such tasks.

549 Moreover, we believe that our insights into the importance of positional encodings for visual reasoning  
 550 tasks have implications beyond ARC, particularly for applications such as physical reasoning in  
 551 vision generation tasks. In these contexts, accurate spatial relationships are equally critical, and our  
 552 findings provide a foundation for further exploration of how Vision Transformers can be adapted to  
 553 meet these challenges.

554 It is important to note that ViTARC solves task-specific instances of ARC in a data-driven approach,  
 555 treating each ARC task independently. This method does not fully solve ARC, which requires the  
 556 ability to generalize across different tasks—a challenge that remains open for future research. How-  
 557 ever, since the current state-of-the-art (SOTA) in ARC relies on LLM-based transduction models  
 558 that handle tasks through supervised input-output transformations (arcprize, 2024), integrating the  
 559 2D inductive bias from ViTARC could provide an orthogonal benefit. This is especially relevant as  
 560 prior studies indicate that the sequential nature of 1D methods in LLMs can limit ARC performance;  
 561 for example, because the input grid is processed in raster order, LLMs experience a significant drop  
 562 in success rates when horizontal movement/filling tasks are rotated 90 degrees (Xu et al., 2024).

563 In summary, this work highlights the importance of 2D positional information and object-based en-  
 564 codings in abstract visual reasoning that leads to our novel contribution of the ViTARC architecture.  
 565 ViTARC advances the application of Vision Transformers for pixel-level reasoning and suggests  
 566 further avenues for improving generalization capabilities in models tackling visual reasoning tasks.

567  
 568  
 569  
 570  
 571  
 572  
 573  
 574  
 575  
 576  
 577  
 578  
 579  
 580  
 581  
 582  
 583  
 584  
 585  
 586  
 587  
 588  
 589  
 590  
 591  
 592  
 593

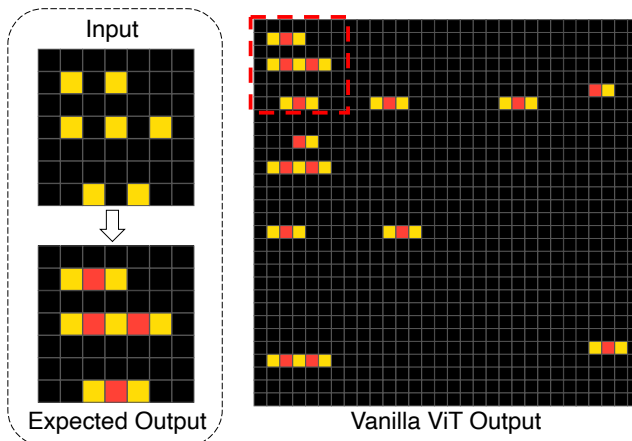
594 REFERENCES  
595

- 596 Josh Achiam, Steven Adler, Sandhini Agarwal, Lama Ahmad, Ilge Akkaya, Florencia Leoni Ale-  
597 man, Diogo Almeida, Janko Altenschmidt, Sam Altman, Shyamal Anadkat, et al. Gpt-4 technical  
598 report. *arXiv preprint arXiv:2303.08774*, 2023.
- 599 James Ainooson, Deepayan Sanyal, Joel P Michelson, Yuan Yang, and Maithilee Kunda. A  
600 neurodiversity-inspired solver for the abstraction\& reasoning corpus (arc) using visual imagery  
601 and program synthesis. *arXiv preprint arXiv:2302.09425*, 2023.
- 602 Simon Alford, Anshula Gandhi, Akshay Rangamani, Andrzej Banburski, Tony Wang, Sylee Dan-  
603 dekar, John Chin, Tomaso Poggio, and Peter Chin. Neural-guided, bidirectional program search  
604 for abstraction and reasoning. In *International Conference on Complex Networks and Their Ap-*  
605 *plications*, pp. 657–668. Springer, 2021.
- 606 Stanislaw Antol, Aishwarya Agrawal, Jiasen Lu, Margaret Mitchell, Dhruv Batra, C. Lawrence Zit-  
607 nick, and Devi Parikh. Vqa: Visual question answering. In *Proceedings of the IEEE International*  
608 *Conference on Computer Vision (ICCV)*, December 2015.
- 609 arcprize. Arc-agri 2024 high scores. <https://arcprize.org/leaderboard>, 2024.
- 610 Rim Assouel, Pau Rodriguez, Perouz Taslakian, David Vazquez, and Yoshua Bengio. Object-centric  
611 compositional imagination for visual abstract reasoning. In *ICLR2022 Workshop on the Elements*  
612 *of Reasoning: Objects, Structure and Causality*, 2022. URL [https://openreview.net/](https://openreview.net/forum?id=rCzfIruU5x5)  
613 forum?id=rCzfIruU5x5.
- 614 Anton Bakhtin, Laurens van der Maaten, Justin Johnson, Laura Gustafson, and Ross Girshick.  
615 Phyre: A new benchmark for physical reasoning. *Advances in Neural Information Processing*  
616 *Systems*, 32, 2019.
- 617 Shraddha Barke, Emmanuel Anaya Gonzalez, Saketh Ram Kasibatla, Taylor Berg-Kirkpatrick, and  
618 Nadia Polikarpova. Hysynth: Context-free llm approximation for guiding program synthesis.  
619 *arXiv preprint arXiv:2405.15880*, 2024.
- 620 G. Bradski. The OpenCV Library. *Dr. Dobb's Journal of Software Tools*, 2000. URL [https://docs.opencv.org/3.4/d4/d73/tutorial\\_py\\_contours\\_begin.html](https://docs.opencv.org/3.4/d4/d73/tutorial_py_contours_begin.html).
- 621 Tom B. Brown, Benjamin Mann, Nick Ryder, Melanie Subbiah, Jared Kaplan, Prafulla Dhari-  
622 wal, Arvind Neelakantan, Pranav Shyam, Girish Sastry, Amanda Askell, Sandhini Agar-  
623 wal, Ariel Herbert-Voss, Gretchen Krueger, Tom Henighan, Rewon Child, Aditya Ramesh,  
624 Daniel M. Ziegler, Jeff Wu, Clemens Winter, Christopher Hesse, Mark Chen, Eric Sigler,  
625 Mateusz Litwin, Scott Gray, Benjamin Chess, Jack Clark, Christopher Berner, Sam Mc-  
626 Candlish, Alec Radford, Ilya Sutskever, and Dario Amodei. Language models are few-shot  
627 learners. *ArXiv*, abs/2005.14165, 2020. URL <https://api.semanticscholar.org/>  
628 CorpusID:218971783.
- 629 Natasha Butt, Blazej Manczak, Auke Wiggers, Corrado Rainone, David W. Zhang, Michaël Def-  
630 ferrard, and Taco Cohen. Codeit: Self-improving language models with prioritized hindsight  
631 replay. In *Forty-first International Conference on Machine Learning*, 2024. URL <https://openreview.net/forum?id=SXVn5IFsrs>.
- 632 Giacomo Camposampiero, Loïc Houmaré, Benjamin Estermann, Joël Mathys, and Roger Wat-  
633 tenhofer. Abstract visual reasoning enabled by language. In *2023 IEEE/CVF Conference on*  
634 *Computer Vision and Pattern Recognition Workshops (CVPRW)*, pp. 2643–2647, 2023. doi:  
635 10.1109/CVPRW59228.2023.00264.
- 636 François Chollet. On the measure of intelligence. *arXiv preprint arXiv:1911.01547*, 2019.
- 637 François Chollet, Katherine Tong, Walter Reade, and Julia Elliott. Ab-  
638 straction and reasoning challenge. [https://www.kaggle.com/c/](https://www.kaggle.com/c/abstraction-and-reasoning-challenge)  
639 abstraction-and-reasoning-challenge, 2020.

- 648 Jack Cole and Mohamed Osman. Dataset-induced meta-learning (and other  
 649 tricks): Improving model efficiency on arc. [https://lab42.global/  
 650 community-model-efficiency/](https://lab42.global/community-model-efficiency/), 2023.
- 651
- 652 Jacob Devlin, Ming-Wei Chang, Kenton Lee, and Kristina Toutanova. Bert: Pre-training of deep  
 653 bidirectional transformers for language understanding. In *North American Chapter of the Association  
 654 for Computational Linguistics*, 2019. URL [https://api.semanticscholar.org/  
 655 CorpusID:52967399](https://api.semanticscholar.org/CorpusID:52967399).
- 656 Alexey Dosovitskiy, Lucas Beyer, Alexander Kolesnikov, Dirk Weissenborn, Xiaohua Zhai, Thomas  
 657 Unterthiner, Mostafa Dehghani, Matthias Minderer, Georg Heigold, Sylvain Gelly, Jakob Uszkoreit,  
 658 and Neil Houlsby. An image is worth 16x16 words: Transformers for image recogni-  
 659 tion at scale. In *International Conference on Learning Representations*, 2021. URL <https://openreview.net/forum?id=YicbFdNTTy>.
- 660
- 661 Sébastien Ferré. First steps of an approach to the arc challenge based on descriptive grid models and  
 662 the minimum description length principle. *arXiv preprint arXiv:2112.00848*, 2021.
- 663
- 664 Raphael Fischer, Matthias Jakobs, Sascha Mücke, and Katharina Morik. Solving abstract reasoning  
 665 tasks with grammatical evolution. In *LWDA*, pp. 6–10, 2020.
- 666
- 667 Martin Gardner and Dana Scott Richards. The colossal book of short puzzles and problems: combi-  
 668 natorics, probability, algebra, geometry, topology, chess, logic, cryptarithms, wordplay, physics  
 669 and other topics of recreational mathematics. (*No Title*), 2006.
- 670 Ryan Greenblatt. Getting 50%(sota) on arc-agi with gpt-4o, Jun  
 671 2024. URL [https://redwoodresearch.substack.com/p/  
 672 getting-50-sota-on-arc-agи-with-gpt](https://redwoodresearch.substack.com/p/getting-50-sota-on-arc-agи-with-gpt).
- 673
- 674 Michael Hahn. Theoretical limitations of self-attention in neural sequence models. *Transactions of  
 675 the Association for Computational Linguistics*, 8:156–171, 2020.
- 676
- 677 Kai Han, Yunhe Wang, Hanting Chen, Xinghao Chen, Jianyuan Guo, Zhenhua Liu, Yehui Tang,  
 678 An Xiao, Chunjing Xu, Yixing Xu, Zhaohui Yang, Yiman Zhang, and Dacheng Tao. A survey  
 679 on vision transformer. *IEEE Transactions on Pattern Analysis and Machine Intelligence*, 45(1):  
 680 87–110, 2023. doi: 10.1109/TPAMI.2022.3152247.
- 681
- 682 Jakob Drachmann Havtorn, Amélie Royer, Tijmen Blankevoort, and Babak Ehteshami Bejnordi.  
 683 Msvit: Dynamic mixed-scale tokenization for vision transformers. In *2023 IEEE/CVF Interna-  
 684 tional Conference on Computer Vision Workshops (ICCVW)*, pp. 838–848, 2023. doi:  
 10.1109/ICCVW60793.2023.00091.
- 685
- 686 Céline Hocquette and Andrew Cropper. Relational decomposition for program synthesis. *arXiv  
 687 preprint arXiv:2408.12212*, 2024.
- 688
- 689 Michael Hodel. Addressing the abstraction and reasoning corpus via procedural example generation.  
*arXiv preprint arXiv:2404.07353*, 2024.
- 690
- 691 Justin Johnson, Bharath Hariharan, Laurens Van Der Maaten, Li Fei-Fei, C Lawrence Zitnick, and  
 692 Ross Girshick. Clevr: A diagnostic dataset for compositional language and elementary visual  
 693 reasoning. In *Proceedings of the IEEE conference on computer vision and pattern recognition*,  
 694 pp. 2901–2910, 2017.
- 695
- 696 Samira Ebrahimi Kahou, Vincent Michalski, Adam Atkinson, Ákos Kádár, Adam Trischler, and  
 697 Yoshua Bengio. Figureqa: An annotated figure dataset for visual reasoning. In *6th International  
 698 Conference on Learning Representations, Workshop Track Proceedings*, 2018.
- 699
- 700 Manoj Kumar, Dirk Weissenborn, and Nal Kalchbrenner. Colorization transformer. In *International  
 701 Conference on Learning Representations*.
- 702 Lab42, Dec 2023. URL [https://lab42.global/past-challenges/  
 703 2023-arcathon/](https://lab42.global/past-challenges/2023-arcathon/).

- 702 Hosung Lee, Sejin Kim, Seungpil Lee, Sanha Hwang, Jihwan Lee, Byung-Jun Lee, and Sundong  
 703 Kim. Arcle: The abstraction and reasoning corpus learning environment for reinforcement learn-  
 704 ing. *arXiv preprint arXiv:2407.20806*, 2024.
- 705 Chao Lei, Nir Lipovetzky, and Krista A Ehinger. Generalized planning for the abstraction and  
 706 reasoning corpus. In *Proceedings of the AAAI Conference on Artificial Intelligence*, volume 38,  
 707 pp. 20168–20175, 2024.
- 708 Shanda Li, Chong You, Guru Guruganesh, Joshua Ainslie, Santiago Ontanon, Manzil Zaheer, Sumit  
 709 Sanghai, Yiming Yang, Sanjiv Kumar, and Srinadh Bhojanapalli. Functional interpolation for  
 710 relative positions improves long context transformers. In *The Twelfth International Conference  
 711 on Learning Representations*.
- 712 Wenbo Li, Zhe Lin, Kun Zhou, Lu Qi, Yi Wang, and Jiaya Jia. Mat: Mask-aware transformer for  
 713 large hole image inpainting. In *Proceedings of the IEEE/CVF Conference on Computer Vision  
 714 and Pattern Recognition (CVPR)*, pp. 10758–10768, June 2022.
- 715 Xiaochuan Li, Baoyu Fan, Runze Zhang, Liang Jin, Di Wang, Zhenhua Guo, Yaqian Zhao, and Ren-  
 716 gang Li. Image content generation with causal reasoning. In *Proceedings of the AAAI Conference  
 717 on Artificial Intelligence*, volume 38, pp. 13646–13654, 2024.
- 718 Jingyun Liang, Jiezheng Cao, Guolei Sun, Kai Zhang, Luc Van Gool, and Radu Timofte. Swinir:  
 719 Image restoration using swin transformer. In *Proceedings of the IEEE/CVF International Confer-  
 720 ence on Computer Vision (ICCV) Workshops*, pp. 1833–1844, October 2021.
- 721 Ze Liu, Yutong Lin, Yue Cao, Han Hu, Yixuan Wei, Zheng Zhang, Stephen Lin, and Baining Guo.  
 722 Swin transformer: Hierarchical vision transformer using shifted windows. In *Proceedings of the  
 723 IEEE/CVF international conference on computer vision*, pp. 10012–10022, 2021.
- 724 Mikołaj Małkiński and Jacek Mańdziuk. A review of emerging research directions in abstract visual  
 725 reasoning. *Information Fusion*, 91:713–736, 2023.
- 726 John Chong Min Tan and Mehul Motani. Llms as a system of multiple expert agents: An approach to  
 727 solve the abstraction and reasoning corpus (arc) challenge. In *2024 IEEE Conference on Artificial  
 728 Intelligence (CAI)*, pp. 782–787, 2024. doi: 10.1109/CAI59869.2024.00149.
- 729 Suvir Mirchandani, Fei Xia, Pete Florence, brian ichter, Danny Driess, Montserrat Gonzalez Arenas,  
 730 Kanishka Rao, Dorsa Sadigh, and Andy Zeng. Large language models as general pattern ma-  
 731 chines. In *7th Annual Conference on Robot Learning*, 2023. URL <https://openreview.net/forum?id=RcZMI8MSyE>.
- 732 Melanie Mitchell, Alessandro B. Palmarini, and Arsenii Kirillovich Moskvichev. Comparing hu-  
 733 mans, GPT-4, and GPT-4v on abstraction and reasoning tasks. In *AAAI 2024 Workshop on "Are  
 734 Large Language Models Simply Causal Parrots?"*, 2023. URL <https://openreview.net/forum?id=3rGT5OkzpC>.
- 735 Arsenii Kirillovich Moskvichev, Victor Vikram Odouard, and Melanie Mitchell. The conceptARC  
 736 benchmark: Evaluating understanding and generalization in the ARC domain. *Transactions on  
 737 Machine Learning Research*, 2023. ISSN 2835-8856. URL <https://openreview.net/forum?id=8ykyGbtt2q>.
- 738 Jaehyun Park, Jaegyun Im, Sanha Hwang, Mintaek Lim, Sabina Ualibekova, Sejin Kim, and Sun-  
 739 dong Kim. Unraveling the arc puzzle: Mimicking human solutions with object-centric decision  
 740 transformer. In *Interactive Learning with Implicit Human Feedback Workshop at ICML 2023*,  
 741 2023.
- 742 Ofir Press, Noah A Smith, and Mike Lewis. Train short, test long: Attention with linear biases  
 743 enables input length extrapolation. *arXiv preprint arXiv:2108.12409*, 2021.
- 744 Colin Raffel, Noam Shazeer, Adam Roberts, Katherine Lee, Sharan Narang, Michael Matena, Yanqi  
 745 Zhou, Wei Li, and Peter J. Liu. Exploring the limits of transfer learning with a unified text-to-  
 746 text transformer. *Journal of Machine Learning Research*, 21(140):1–67, 2020. URL <http://jmlr.org/papers/v21/20-074.html>.

- 756 Jean Raven. Raven progressive matrices. In *Handbook of nonverbal assessment*, pp. 223–237.  
 757 Springer, 2003.
- 758
- 759 Peter Shaw, Jakob Uszkoreit, and Ashish Vaswani. Self-attention with relative position represen-  
 760 tations. In Marilyn Walker, Heng Ji, and Amanda Stent (eds.), *Proceedings of the 2018 Con-  
 761 ference of the North American Chapter of the Association for Computational Linguistics: Hu-  
 762 man Language Technologies, Volume 2 (Short Papers)*, pp. 464–468, New Orleans, Louisiana,  
 763 June 2018. Association for Computational Linguistics. doi: 10.18653/v1/N18-2074. URL  
<https://aclanthology.org/N18-2074>.
- 764
- 765 Jianlin Su, Murtadha Ahmed, Yu Lu, Shengfeng Pan, Wen Bo, and Yunfeng Liu. Roformer: En-  
 766 hanced transformer with rotary position embedding. *Neurocomputing*, 568:127063, 2024.
- 767
- 768 Hugo Touvron, Matthieu Cord, Matthijs Douze, Francisco Massa, Alexandre Sablayrolles, and  
 769 Hervé Jégou. Training data-efficient image transformers & distillation through attention. In  
 770 *International conference on machine learning*, pp. 10347–10357. PMLR, 2021.
- 771
- 772 Ashish Vaswani, Noam M. Shazeer, Niki Parmar, Jakob Uszkoreit, Llion Jones, Aidan N. Gomez,  
 773 Lukasz Kaiser, and Illia Polosukhin. Attention is all you need. In *Neural Information Processing  
 Systems*, 2017. URL <https://api.semanticscholar.org/CorpusID:13756489>.
- 774
- 775 Ruocheng Wang, Eric Zelikman, Gabriel Poesia, Yewen Pu, Nick Haber, and Noah Goodman. Hy-  
 776 pothesis search: Inductive reasoning with language models. In *The Twelfth International Confer-  
 777 ence on Learning Representations*, 2024. URL <https://openreview.net/forum?id=G7UtIGQmjm>.
- 778
- 779 Zhendong Wang, Xiaodong Cun, Jianmin Bao, Wengang Zhou, Jianzhuang Liu, and Houqiang Li.  
 780 Uformer: A general u-shaped transformer for image restoration. In *Proceedings of the IEEE/CVF  
 conference on computer vision and pattern recognition*, pp. 17683–17693, 2022.
- 781
- 782 Jason Wei, Xuezhi Wang, Dale Schuurmans, Maarten Bosma, Fei Xia, Ed Chi, Quoc V Le, Denny  
 783 Zhou, et al. Chain-of-thought prompting elicits reasoning in large language models. *Advances in  
 784 neural information processing systems*, 35:24824–24837, 2022.
- 785
- 786 J S Wind. 1st place solution + code and official documentation. <https://www.kaggle.com/competitions/abstraction-and-reasoning-challenge/discussion/154597>, 2020.
- 787
- 788
- 789 Kan Wu, Houwen Peng, Minghao Chen, Jianlong Fu, and Hongyang Chao. Rethinking and improv-  
 790 ing relative position encoding for vision transformer. In *Proceedings of the IEEE/CVF Interna-  
 791 tional Conference on Computer Vision (ICCV)*, pp. 10033–10041, October 2021.
- 792
- 793 Yudong Xu, Elias B Khalil, and Scott Sanner. Graphs, constraints, and search for the abstraction and  
 794 reasoning corpus. In *Proceedings of the AAAI Conference on Artificial Intelligence*, volume 37,  
 795 pp. 4115–4122, 2023.
- 796
- 797 Yudong Xu, Wenhao Li, Pashootan Vaezipoor, Scott Sanner, and Elias Boutros Khalil. LLMs and  
 798 the abstraction and reasoning corpus: Successes, failures, and the importance of object-based  
 799 representations. *Transactions on Machine Learning Research*, 2024. ISSN 2835-8856. URL  
<https://openreview.net/forum?id=E8m8oySvPJ>.
- 800
- 801 Rowan Zellers, Yonatan Bisk, Ali Farhadi, and Yejin Choi. From recognition to cognition: Visual  
 802 commonsense reasoning. In *Proceedings of the IEEE/CVF Conference on Computer Vision and  
 Pattern Recognition (CVPR)*, June 2019.
- 803
- 804 Qiqi Zhou and Yichen Zhu. Make a long image short: Adaptive token length for vision transformers.  
 805 In *Joint European Conference on Machine Learning and Knowledge Discovery in Databases*, pp.  
 806 69–85. Springer, 2023.
- 807
- 808 Yongchao Zhou, Uri Alon, Xinyun Chen, Xuezhi Wang, Rishabh Agarwal, and Denny Zhou.  
 809 Transformers can achieve length generalization but not robustly. In *ICLR 2024 Workshop  
 on Mathematical and Empirical Understanding of Foundation Models*, 2024. URL <https://openreview.net/forum?id=DWkWIh3vFJ>.

810 A VANILLA ViT FAILURE ANALYSIS  
811

828 Figure 8: **Failure case of ViT-Vanilla with NLP <pad> tokens.** ViT-Vanilla with 2D padding and  
829 NLP <pad> tokens fails to account for the actual inner grid size, filling the entire  $h_{\max} \times w_{\max}$  space.  
830 When the output is cropped to the true grid dimensions, the predictions within the valid region  
831 are correct, underscoring the importance of proper boundary handling.

832  
833 B TRAINING DETAILS  
834

835 This section provides a comprehensive overview of the training setup, including hyperparameters,  
836 hardware specifications, and other relevant details regarding the training process.

837 Our model consists of 3 layers with 8 attention heads and a hidden dimension of 128. The model  
838 was trained on various single-core GPU nodes, including P100, V100, and T4, with a batch size of  
839 8 for 1 epoch. The typical training time per task ranges from 6 to 10 hours (wall clock).

840 The dataset was generated using Hodel’s generators (Hodel, 2024), producing 1 million samples,  
841 which were then split into training, validation, and test sets with 998,000, 1,000, and 1,000 instances,  
842 respectively. The generation time varies between 3 and 12 hours, depending on the task.  
843 A fixed random seed (1230) was used for both dataset generation and model training to ensure  
844 reproducibility.

845 Due to computational resource constraints, the ablation study was performed on a randomly sampled  
846 subset of 100 tasks from the total 400, also selected using seed 1230.

847  
848 C FULL RESULTS FOR TASK-SPECIFIC ACCURACIES  
849850 C.1 MAIN MODELS ON FULL 400 TASKS  
851

852 Table 1: Solved Test Instances (%) Across Models on all 400 tasks.

853 Model	854 Solved Test Instances (%)			
	855 Mean	856 Med.	857 25th Pctl.	858 75th Pctl.
859 Baseline (ViT-Vanilla)	17.68	3.20	0.10	22.85
860 ViTARC-VT	66.03	87.85	27.55	99.30
861 ViTARC (Full Model)	75.04	95.10	58.07	99.80

864

865

866

867

Table 2: Model accuracies across tasks (100/400)

868

869

Task	ViT -Vanilla	ViTARC -VT	ViTARC	Task	ViT -Vanilla	ViTARC -VT	ViTARC
ce22a75a	0.00	0.94	1.00	444801d8	0.00	0.98	1.00
1f876c06	0.00	0.99	1.00	b27ca6d3	0.00	0.99	1.00
68b16354	0.00	0.99	1.00	2c608aff	0.00	1.00	1.00
d037b0a7	0.00	1.00	1.00	0ca9ddb6	0.00	1.00	1.00
543a7ed5	0.00	1.00	1.00	952a094c	0.00	1.00	1.00
af902bf9	0.00	1.00	1.00	49d1d64f	0.00	1.00	1.00
0962bcdd	0.00	1.00	1.00	d364b489	0.00	1.00	1.00
b60334d2	0.00	1.00	1.00	a9f96cdd	0.00	1.00	1.00
95990924	0.00	1.00	1.00	54d82841	0.00	0.80	0.99
25d487eb	0.00	0.95	0.99	5c0a986e	0.00	0.96	0.99
d687bc17	0.00	0.97	0.99	363442ee	0.00	0.98	0.99
6cdd2623	0.00	0.98	0.99	db93a21d	0.00	0.93	0.97
5168d44c	0.00	0.94	0.97	3befdf3e	0.00	0.97	0.97
22233c11	0.00	0.97	0.97	67a3c6ac	0.00	1.00	0.97
ae3edfdc	0.00	0.72	0.96	ded97339	0.00	0.92	0.96
a2fd1cf0	0.00	0.95	0.96	d4a91cb9	0.00	0.98	0.96
d4f3cd78	0.00	0.99	0.96	6cf79266	0.00	0.96	0.95
e98196ab	0.00	0.99	0.95	56ff96f3	0.00	0.90	0.94
694f12f3	0.00	0.91	0.94	93b581b8	0.00	0.99	0.94
39e1d7f9	0.00	0.42	0.93	8403a5d5	0.00	1.00	0.93
ecdecbb3	0.00	0.76	0.92	31aa019c	0.00	0.82	0.90
ec883f72	0.00	0.87	0.90	36fdfd69	0.00	0.75	0.89
b7249182	0.00	0.74	0.88	e9614598	0.00	0.86	0.88
e76a88a6	0.00	0.00	0.87	3ac3eb23	0.00	0.71	0.87
a64e4611	0.00	0.98	0.87	50846271	0.00	0.84	0.86
928ad970	0.00	0.97	0.86	40853293	0.00	0.99	0.86
6ecd11f4	0.00	0.00	0.84	b527c5c6	0.00	0.66	0.84
1e0a9b12	0.00	0.69	0.84	7ddcd7ec	0.00	0.75	0.84
2013d3e2	0.00	0.95	0.84	e50d258f	0.00	0.70	0.83
1caeab9d	0.00	0.42	0.82	5ad4f10b	0.00	0.62	0.82
98cf29f8	0.00	0.66	0.82	264363fd	0.00	0.79	0.82
5521c0d9	0.00	0.75	0.79	0a938d79	0.00	0.86	0.78
f8a8fe49	0.00	0.68	0.74	a48eeaf7	0.00	0.76	0.73
aba27056	0.00	0.59	0.70	2bcee788	0.00	0.64	0.70
47c1f68c	0.00	0.45	0.68	b548a754	0.00	0.95	0.68
890034e9	0.00	0.59	0.67	508bd3b6	0.00	0.66	0.64
6aa20dc0	0.00	0.33	0.63	2dd70a9a	0.00	0.33	0.59
7c008303	0.00	0.48	0.58	6d58a25d	0.00	0.33	0.56
f8c80d96	0.00	0.13	0.55	6855a6e4	0.00	0.44	0.51
4093f84a	0.00	0.31	0.49	90c28cc7	0.00	0.42	0.48
db3e9e38	0.00	0.34	0.47	05f2a901	0.00	0.04	0.46
5c2c9af4	0.00	0.51	0.46	d06dbe63	0.00	0.57	0.46
5daaa586	0.00	0.17	0.43	f1cefba8	0.00	0.19	0.43
3906de3d	0.00	0.28	0.42	caa06a1f	0.00	0.19	0.41
75b8110e	0.00	0.62	0.40	e8dc4411	0.00	0.28	0.39
8731374e	0.00	0.22	0.38	e48d4e1a	0.00	0.30	0.38
f35d900a	0.00	0.65	0.38	f15e1fac	0.00	0.10	0.37
6e19193c	0.00	0.12	0.37	3de23699	0.00	0.00	0.35
6b9890af	0.00	0.00	0.35	a78176bb	0.00	0.26	0.32
1b60fb0c	0.00	0.14	0.28	e509e548	0.00	0.02	0.27

916

917

918  
919  
920

921 Table 3: Model accuracies across tasks (200/400)

Task	ViT -Vanilla	ViTARC -VT	ViTARC	Task	ViT -Vanilla	ViTARC -VT	ViTARC
a1570a43	0.00	0.54	0.25	3e980e27	0.00	0.02	0.22
88a10436	0.00	0.00	0.20	9aec4887	0.00	0.02	0.19
7df24a62	0.00	0.10	0.19	e21d9049	0.00	0.10	0.19
8a004b2b	0.00	0.02	0.18	1f0c79e5	0.00	0.14	0.16
045e512c	0.00	0.06	0.14	ce602527	0.00	0.00	0.12
b775ac94	0.00	0.03	0.12	8eb1be9a	0.00	0.03	0.07
fcb5c309	0.00	0.00	0.06	a61ba2ce	0.00	0.00	0.06
36d67576	0.00	0.04	0.06	846bdb03	0.00	0.00	0.05
234bbc79	0.00	0.00	0.05	e40b9e2f	0.00	0.02	0.05
57aa92db	0.00	0.03	0.05	5117e062	0.00	0.00	0.04
8efcae92	0.00	0.00	0.04	72322fa7	0.00	0.02	0.04
623ea044	0.00	0.02	0.04	4938f0c2	0.00	0.07	0.04
3bd67248	0.00	0.08	0.04	48d8fb45	0.00	0.00	0.03
a87f7484	0.00	0.00	0.03	447fd412	0.00	0.01	0.03
e6721834	0.00	0.01	0.03	4c5c2cf0	0.00	0.08	0.03
be94b721	0.00	0.00	0.02	a8c38be5	0.00	0.00	0.02
d07ae81c	0.00	0.00	0.01	97a05b5b	0.00	0.01	0.01
99b1bc43	0.00	0.00	0.00	137eaa0f	0.00	0.00	0.00
c8cbb738	0.00	0.00	0.00	e5062a87	0.00	0.00	0.00
60b61512	0.01	0.83	1.00	e8593010	0.01	0.83	1.00
a79310a0	0.01	0.98	1.00	d43fd935	0.01	0.98	1.00
253bf280	0.01	0.99	1.00	dbc1a6ce	0.01	1.00	1.00
4c4377d9	0.01	1.00	1.00	8be77c9e	0.01	1.00	1.00
77fdfe62	0.01	1.00	1.00	ed36ccf7	0.01	1.00	1.00
25ff71a9	0.01	1.00	1.00	f5b8619d	0.01	1.00	1.00
dc1df850	0.01	1.00	1.00	10fc当地3	0.01	0.99	0.99
178fcbfb	0.01	1.00	0.99	3428a4f5	0.01	0.79	0.98
11852cab	0.01	0.92	0.98	4612dd53	0.01	0.96	0.98
fcc82909	0.01	0.96	0.97	dc433765	0.01	0.91	0.96
39a8645d	0.01	0.01	0.94	6fa7a44f	0.01	1.00	0.94
834ec97d	0.01	0.94	0.93	321b1fc6	0.01	0.55	0.92
4522001f	0.01	0.22	0.88	88a62173	0.01	0.97	0.85
d9f24cd1	0.01	0.67	0.74	a65b410d	0.01	0.69	0.74
9edfc990	0.01	0.33	0.48	6455b5f5	0.01	0.22	0.27
72ca375d	0.01	0.01	0.14	3f7978a0	0.01	0.04	0.14
f9012d9b	0.01	0.02	0.02	0e206a2e	0.01	0.02	0.02
a8d7556c	0.02	0.93	1.00	74dd1130	0.02	1.00	1.00
d13f3404	0.02	1.00	1.00	6d0aefbc	0.02	1.00	1.00
c9e6f938	0.02	1.00	1.00	913fb3ed	0.02	1.00	1.00
41e4d17e	0.02	0.83	0.99	94f9d214	0.02	0.74	0.96
83302e8f	0.02	0.75	0.94	b94a9452	0.02	0.45	0.85
1f85a75f	0.02	0.03	0.81	b6afb2da	0.02	1.00	0.77
6e82a1ae	0.02	0.24	0.63	00d62c1b	0.02	0.46	0.63
82819916	0.02	0.20	0.60	63613498	0.02	0.02	0.16
228f6490	0.02	0.03	0.06	09629e4f	0.02	0.02	0.03
6d75e8bb	0.03	0.99	1.00	bc1d5164	0.03	1.00	1.00
bdad9b1f	0.03	1.00	1.00	eb281b96	0.03	1.00	1.00
e26a3af2	0.03	0.92	0.99	8d510a79	0.03	0.99	0.99
f2829549	0.03	0.89	0.98	6430c8c4	0.03	0.89	0.98
f25fbde4	0.03	0.02	0.96	fafffa47	0.03	0.92	0.94

970  
971

972  
973  
974

975 Table 4: Model accuracies across tasks (300/400)

976 Task	977 ViT -Vanilla	ViTARC -VT	ViTARC	978 Task	979 ViT -Vanilla	980 ViTARC -VT	981 ViTARC
6773b310	0.03	0.78	0.91	a740d043	0.03	0.84	0.84
56dc2b01	0.03	0.43	0.58	d2abd087	0.03	0.09	0.15
681b3aeb	0.03	0.04	0.05	5bd6f4ac	0.04	1.00	1.00
8d5021e8	0.04	1.00	1.00	3c9b0459	0.04	1.00	1.00
6150a2bd	0.04	1.00	1.00	62c24649	0.04	1.00	0.99
3af2c5a8	0.04	1.00	0.99	1a07d186	0.04	0.84	0.98
855e0971	0.04	0.96	0.98	4258a5f9	0.04	0.97	0.98
3aa6fb7a	0.04	1.00	0.98	6d0160f0	0.04	0.03	0.97
29ec7d0e	0.04	0.62	0.83	ae4f1146	0.04	0.14	0.67
760b3cac	0.04	0.66	0.64	29623171	0.04	0.37	0.44
673ef223	0.04	0.30	0.26	2281f1f4	0.05	1.00	1.00
cf98881b	0.05	1.00	1.00	ce4f8723	0.05	0.97	0.99
6c434453	0.05	0.93	0.96	c1d99e64	0.05	0.99	0.95
2dc579da	0.05	0.38	0.69	c909285e	0.05	0.20	0.58
73251a56	0.05	0.66	0.39	776ffc46	0.05	0.03	0.16
3345333e	0.05	0.08	0.14	beb8660c	0.05	0.09	0.09
80af3007	0.06	0.98	1.00	7f4411dc	0.06	0.95	0.99
32597951	0.06	0.98	0.99	7468f01a	0.06	0.42	0.84
810b9b61	0.06	0.70	0.82	a5313dff	0.06	0.61	0.76
ef135b50	0.07	0.99	1.00	dae9d2b5	0.07	0.95	0.97
1c786137	0.07	0.05	0.75	d8c310e9	0.07	0.72	0.74
d22278a0	0.07	0.70	0.66	d0f5fe59	0.08	0.09	1.00
d5d6de2d	0.08	0.98	1.00	a416b8f3	0.08	1.00	1.00
1f642eb9	0.08	1.00	1.00	c444b776	0.08	0.96	0.99
cbded52d	0.08	0.97	0.97	780d0b14	0.08	0.97	0.96
0b148d64	0.08	0.26	0.62	b782dc8a	0.08	0.30	0.28
9f236235	0.09	0.98	0.88	0dfd9992	0.09	0.67	0.84
7837ac64	0.09	0.82	0.82	aabf363d	0.09	0.12	0.73
b8cdaf2b	0.09	0.64	0.61	a61f2674	0.10	0.75	0.84
ce9e57f2	0.10	0.75	0.83	7b6016b9	0.10	0.65	0.80
0520fde7	0.11	1.00	1.00	496994bd	0.11	1.00	0.97
150deff5	0.11	0.91	0.95	25d8a9c8	0.12	0.46	1.00
1b2d62fb	0.12	0.99	1.00	1bfc4729	0.12	1.00	1.00
3618c87e	0.12	0.98	0.99	90f3ed37	0.12	0.83	0.84
484b58aa	0.12	0.54	0.66	662c240a	0.12	0.77	0.42
b2862040	0.12	0.30	0.39	d90796e8	0.13	1.00	1.00
6a1e5592	0.13	0.18	0.22	42a50994	0.14	0.98	1.00
2bee17df	0.14	0.99	1.00	67e8384a	0.14	1.00	1.00
017c7c7b	0.14	0.95	0.99	a3325580	0.14	0.01	0.00
ddf7fa4f	0.15	0.78	0.95	23b5c85d	0.16	0.03	0.24
05269061	0.16	0.12	0.22	22168020	0.17	1.00	1.00
23581191	0.17	0.92	0.96	53b68214	0.17	0.94	0.96
7e0986d6	0.18	0.97	1.00	b190f7f5	0.18	0.97	0.98
a3df8b1e	0.18	0.14	0.22	ea786f4a	0.19	0.98	0.98
28bf18c6	0.19	0.07	0.81	3eda0437	0.19	0.68	0.69
22eb0ac0	0.20	0.96	1.00	3631a71a	0.20	0.99	1.00
aedd82e4	0.20	1.00	1.00	025d127b	0.20	1.00	1.00
08ed6ac7	0.20	0.99	0.95	44d8ac46	0.20	0.59	0.86
ff805c23	0.21	0.10	0.28	e179c5f4	0.22	0.01	0.01
1cf80156	0.23	0.12	0.83	f8ff0b80	0.23	0.33	0.65

1024  
1025

1026

1027

1028

1029

Table 5: Model accuracies across tasks (400/400)

Task	ViT -Vanilla	ViTARC -VT	ViTARC	Task	ViT -Vanilla	ViTARC -VT	ViTARC
1fad071e	0.23	0.24	0.59	9ecd008a	0.23	0.16	0.24
67385a82	0.24	1.00	1.00	868de0fa	0.24	1.00	1.00
c9f8e694	0.24	1.00	1.00	d6ad076f	0.24	0.98	0.99
dc0a314f	0.24	0.14	0.24	27a28665	0.26	0.24	0.94
9af7a82c	0.26	0.00	0.00	4290ef0e	0.27	0.24	0.80
539a4f51	0.28	0.72	0.76	cdecee7f	0.28	0.04	0.11
99fa7670	0.29	1.00	1.00	e73095fd	0.29	0.98	0.99
9dfd6313	0.29	0.99	0.99	b0c4d837	0.29	0.21	0.97
963e52fc	0.30	1.00	1.00	941d9a10	0.30	0.98	0.99
b230c067	0.30	0.44	0.46	b9b7f026	0.31	0.37	1.00
06df4c85	0.31	1.00	1.00	67a423a3	0.32	1.00	0.99
54d9e175	0.33	1.00	1.00	28e73c20	0.33	1.00	0.98
6f8cd79b	0.33	1.00	0.98	ea32f347	0.34	0.65	0.71
97999447	0.35	1.00	1.00	a85d4709	0.35	0.00	0.83
a5f85a15	0.36	0.99	1.00	c59eb873	0.36	1.00	1.00
7b7f7511	0.36	0.89	0.95	d10ecb37	0.39	1.00	1.00
d89b689b	0.41	0.96	0.98	de1cd16c	0.41	0.37	0.97
29c11459	0.43	1.00	1.00	9172f3a0	0.43	1.00	1.00
a68b268e	0.44	1.00	1.00	ba97ae07	0.44	1.00	1.00
ff28f65a	0.44	0.70	0.96	1190e5a7	0.44	0.81	0.91
d406998b	0.46	0.98	1.00	ba26e723	0.47	1.00	1.00
f25ffba3	0.50	0.99	1.00	c3f564a4	0.52	0.94	1.00
2204b7a8	0.52	0.96	0.98	272f95fa	0.54	1.00	1.00
91714a58	0.54	0.94	0.98	1e32b0e9	0.56	0.99	1.00
d9fac9be	0.57	0.68	0.97	44f52bb0	0.57	0.55	0.84
d23f8c26	0.59	1.00	1.00	b8825c91	0.60	0.99	0.99
ac0a08a4	0.61	0.99	1.00	bb43febb	0.61	1.00	1.00
c0f76784	0.61	1.00	1.00	e9afc9a	0.62	1.00	0.98
b91ae062	0.64	1.00	1.00	cce03e0d	0.64	1.00	1.00
007bbfb7	0.65	0.99	1.00	91413438	0.65	0.38	0.32
c3e719e8	0.66	0.99	1.00	e3497940	0.66	1.00	1.00
d631b094	0.66	0.41	0.64	50cb2852	0.68	1.00	1.00
8e1813be	0.70	0.99	1.00	9565186b	0.74	0.96	1.00
a699fb00	0.74	1.00	1.00	4347f46a	0.76	1.00	0.99
469497ad	0.76	0.92	0.95	239be575	0.76	0.74	0.82
8f2ea7aa	0.81	0.23	0.98	5614dbc9	0.82	1.00	1.00
9d9215db	0.83	0.96	0.97	85c4e7cd	0.84	0.99	0.90
8e5a5113	0.85	0.98	0.99	46442a0e	0.86	1.00	1.00
7fe24cdd	0.86	1.00	1.00	445eab21	0.86	0.92	0.96
bd4472b8	0.89	0.49	0.58	3bdb4ada	0.92	1.00	1.00
bda2d7a6	0.94	0.98	1.00	f76d97a5	0.94	1.00	1.00
2dee498d	0.95	1.00	1.00	46f33fce	0.96	1.00	1.00
746b3537	0.96	0.99	0.99	eb5a1d5d	0.97	1.00	1.00
0d3d703e	0.98	1.00	1.00	5582e5ca	0.98	0.95	0.99
f8b3ba0a	0.98	0.99	0.97	feca6190	0.98	0.11	0.79
794b24be	0.98	0.24	0.23	d511f180	0.99	1.00	1.00
b1948b0a	0.99	1.00	1.00	c8f0f002	0.99	1.00	1.00
995c5fa3	1.00	0.00	1.00	6e02f1e3	1.00	1.00	1.00
bbc9ae5d	1.00	1.00	1.00	d4469b4b	1.00	1.00	1.00
7447852a	1.00	1.00	1.00	4be741c5	1.00	1.00	1.00

1078

1079

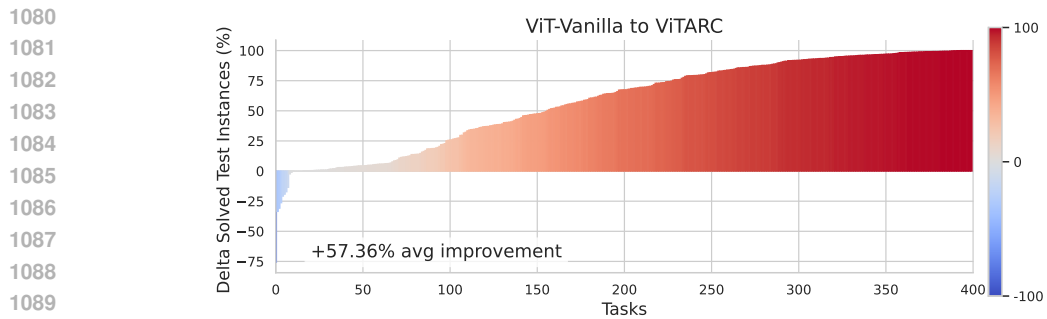


Figure 9: Improvement in percentage of solved test instances per task, from ViT-Vanilla to ViTARC.

## C.2 ABLATION MODELS ON SAMPLED 100 TASKS

Table 6: Solved test instances (%) across models on sampled 100 tasks and ablation of sub-steps. The Delta (Mean) column shows the change in the mean solved instances: the "Border Tokens" is compared to ViTARC-VT, while the three positional encoding ablations (PEmixer, 2D RPE, and OPE) are compared to ViTARC. Note that the numbers for ViT-Vanilla, ViTARC-VT, and ViTARC differ from the 400-task table as these are based on the 100-task subset.

Model	Solved Test Instances (%)				<b>Delta (Mean)</b>
	Mean	Median	25th Pctl.	75th Pctl.	
Baseline (ViT-Vanilla)	15.98	3.65	0.10	15.90	-
ViTARC-VT	67.30	90.00	32.77	99.42	base
- Border Tokens	62.71	79.60	28.62	98.80	-4.59
ViTARC (Full Model)	78.77	95.50	78.20	99.83	base
- Positional Encoding Mixer (PEmixer)	73.03	91.25	54.90	99.05	-5.74
- 2D Relative Positional Encoding (2D RPE)	60.78	73.30	28.85	97.30	-17.99
- Object-based Positional Encoding (OPE)	75.39	95.45	64.22	99.72	-3.38

1110  
1111  
1112  
1113  
1114  
1115  
1116  
1117  
1118  
1119  
1120  
1121  
1122  
1123  
1124  
1125  
1126  
1127  
1128  
1129  
1130  
1131  
1132  
1133

1134  
1135  
1136  
1137

1138 Table 7: Exact Match Scores for each task on 100 sampled tasks across different models and abla-  
1139 tions.

1140	Task	ViT-Vanilla	ViTARC -VT	-BorderTokens	ViTARC	-PEmixer	-RPE	-OPE
1141	0ca9ddb6	0.00	1.00	1.00	1.00	0.27	1.00	1.00
1142	543a7ed5	0.00	1.00	1.00	1.00	1.00	1.00	1.00
1143	952a094c	0.00	1.00	0.98	1.00	0.99	1.00	0.17
1144	49d1d64f	0.00	1.00	1.00	1.00	1.00	1.00	1.00
1145	25d487eb	0.00	0.95	0.99	0.99	0.08	0.95	0.37
1146	d687bc17	0.00	0.97	0.40	0.99	0.38	0.99	0.78
1147	67a3c6ac	0.00	1.00	0.84	0.97	0.99	1.00	1.00
1148	e98196ab	0.00	0.99	0.96	0.95	0.92	1.00	0.09
1149	8403a5d5	0.00	1.00	0.98	0.93	0.72	0.97	0.94
1150	31aa019c	0.00	0.82	0.69	0.90	0.89	0.99	0.81
1151	ec883f72	0.00	0.87	0.87	0.90	0.79	0.95	0.82
1152	b7249182	0.00	0.74	0.61	0.88	0.81	0.90	0.32
1153	e76a88a6	0.00	0.00	0.91	0.87	0.00	0.06	0.00
1154	3ac3eb23	0.00	0.71	0.71	0.87	0.85	0.87	0.57
1155	a64e4611	0.00	0.98	0.97	0.87	0.90	0.99	0.99
1156	40853293	0.00	0.99	0.92	0.86	0.98	0.98	0.96
1157	b527c5c6	0.00	0.66	0.74	0.84	0.56	0.76	0.53
1158	2013d3e2	0.00	0.95	0.92	0.84	0.11	0.94	0.94
1159	1caeab9d	0.00	0.42	0.78	0.82	0.48	0.58	0.36
1160	5521c0d9	0.00	0.75	0.69	0.79	0.76	0.80	0.71
1161	6aa20dc0	0.00	0.33	0.52	0.63	0.38	0.51	0.23
1162	2dd70a9a	0.00	0.33	0.32	0.59	0.35	0.51	0.30
1163	5c2c9af4	0.00	0.51	0.40	0.46	0.53	0.53	0.31
1164	5daaa586	0.00	0.17	0.48	0.43	0.22	0.37	0.12
1165	6e19193c	0.00	0.12	0.18	0.37	0.29	0.08	0.08
1166	1b60fb0c	0.00	0.14	0.17	0.28	0.06	0.12	0.04
1167	9aec4887	0.00	0.02	0.11	0.19	0.01	0.03	0.00
1168	8a004b2b	0.00	0.02	0.10	0.18	0.02	0.11	0.00
1169	1f0c79e5	0.00	0.14	0.06	0.16	0.02	0.29	0.11
1170	a87f7484	0.00	0.00	0.01	0.03	0.00	0.14	0.00
1171	be94b721	0.00	0.00	0.02	0.02	0.01	0.00	0.00
1172	c8ccb738	0.00	0.00	0.01	0.00	0.00	0.01	0.00
1173	e5062a87	0.00	0.00	0.00	0.00	0.00	0.00	0.00
1174	d43fd935	0.01	0.98	0.98	1.00	0.97	0.99	0.99
1175	dbc1a6ce	0.01	1.00	0.92	1.00	0.99	1.00	0.99
1176	dc1df850	0.01	1.00	1.00	1.00	1.00	1.00	1.00
1177	dc433765	0.01	0.91	0.92	0.96	0.68	0.97	0.94
1178	39a8645d	0.01	0.01	0.99	0.94	0.70	0.16	0.01
1179	4522001f	0.01	0.22	0.62	0.88	0.74	0.79	0.76
1180	3f7978a0	0.01	0.04	0.12	0.14	0.06	0.11	0.01
1181	d13f3404	0.02	1.00	1.00	1.00	1.00	1.00	1.00
1182	913fb3ed	0.02	1.00	1.00	1.00	0.98	1.00	0.99
1183	94f9d214	0.02	0.74	0.51	0.96	0.08	0.98	0.93
1184	228f6490	0.02	0.03	0.06	0.06	0.04	0.04	0.02
1185	bdad9b1f	0.03	1.00	1.00	1.00	1.00	1.00	1.0
1186	eb281b96	0.03	1.00	1.00	1.00	1.00	1.00	1.00
1187	6430c8c4	0.03	0.89	0.53	0.98	0.43	0.99	0.96
1188	a740d043	0.03	0.84	0.65	0.84	0.64	0.82	0.46
1189	d2abd087	0.03	0.09	0.12	0.15	0.09	0.11	0.07
1190	5bd6f4ac	0.04	1.00	1.00	1.00	1.00	1.00	1.00

1186  
1187

Table 8: Exact Match Scores for each task on 100 sampled tasks across different models and ablations.

Task	ViT-Vanilla	ViTARC -VT	-BorderTokens	ViTARC	-PEmixer	-RPE	-OPE
8d5021e8	0.04	1.00	1.00	1.00	1.00	0.96	1.00
6150a2bd	0.04	1.00	0.57	1.00	0.69	1.00	1.00
3af2c5a8	0.04	1.00	1.00	0.99	1.00	1.00	0.98
6d0160f0	0.04	0.03	0.93	0.97	0.02	0.98	0.56
29ec7d0e	0.04	0.62	0.69	0.83	0.64	0.88	0.64
760b3cac	0.04	0.66	0.60	0.64	0.11	0.78	0.47
6c434453	0.05	0.93	0.92	0.96	0.41	0.93	0.91
c1d99e64	0.05	0.99	0.92	0.95	0.90	0.95	0.96
2dc579da	0.05	0.38	0.55	0.69	0.43	0.71	0.16
beb8660c	0.05	0.09	0.06	0.09	0.08	0.13	0.06
7f4411dc	0.06	0.95	0.98	0.99	0.90	1.00	0.97
32597951	0.06	0.98	0.98	0.99	0.97	1.00	0.99
1c786137	0.07	0.05	0.76	0.75	0.05	0.80	0.44
d5d6de2d	0.08	0.98	1.00	1.00	0.30	0.99	0.92
1f642eb9	0.08	1.00	0.92	1.00	0.89	1.00	0.98
c444b776	0.08	0.96	0.98	0.99	0.93	0.98	0.82
0dfd9992	0.09	0.67	0.82	0.84	0.73	0.83	0.66
7837ac64	0.09	0.82	0.85	0.82	0.85	0.79	0.60
a61f2674	0.10	0.75	0.71	0.84	0.84	0.86	0.54
ce9e57f2	0.10	0.75	0.80	0.83	0.76	0.71	0.50
b2862040	0.12	0.30	0.35	0.39	0.34	0.39	0.32
d90796e8	0.13	1.00	1.00	1.00	0.85	1.00	1.00
42a50994	0.14	0.98	0.97	1.00	0.82	0.99	0.24
2bee17df	0.14	0.99	1.00	1.00	0.01	1.00	0.98
ddf7fa4f	0.15	0.78	0.87	0.95	0.86	0.81	0.85
7e0986d6	0.18	0.97	1.00	1.00	1.00	0.99	0.99
ea786f4a	0.19	0.98	0.99	0.98	0.39	0.99	0.99
44d8ac46	0.20	0.59	0.70	0.86	0.79	0.74	0.63
868de0fa	0.24	1.00	1.00	1.00	1.00	0.99	1.00
dc0a314f	0.24	0.14	0.24	0.24	0.28	0.35	0.01
9af7a82c	0.26	0.00	0.00	0.00	0.00	0.00	0.00
99fa7670	0.29	1.00	1.00	1.00	0.97	1.00	1.00
b0c4d837	0.29	0.21	0.91	0.97	0.21	0.93	0.13
d89b689b	0.41	0.96	0.97	0.98	0.93	0.98	0.38
de1cd16c	0.41	0.37	0.97	0.97	0.60	0.96	0.38
a68b268e	0.44	1.00	0.93	1.00	1.00	1.00	0.98
d406998b	0.46	0.98	1.00	1.00	0.39	1.00	0.73
c3f564a4	0.52	0.94	0.94	1.00	0.88	1.00	0.92
44f52bb0	0.57	0.55	0.78	0.84	0.66	0.66	0.54
ac0a08a4	0.61	0.99	0.98	1.00	1.00	1.00	1.00
cce03e0d	0.64	1.00	1.00	1.00	1.00	1.00	1.00
007bbfb7	0.65	0.99	1.00	1.00	0.84	1.00	1.00
91413438	0.65	0.38	0.34	0.32	0.33	0.32	0.92
d631b094	0.66	0.41	0.43	0.64	0.64	0.73	0.05
445eab21	0.86	0.92	0.97	0.96	0.92	0.92	0.90
46f33fce	0.96	1.00	1.00	1.00	0.84	1.00	1.00
5582e5ca	0.98	0.95	1.00	0.99	0.98	0.97	0.96
c8f0f002	0.99	1.00	1.00	1.00	1.00	1.00	1.00
995c5fa3	1.00	0.00	1.00	1.00	1.00	0.02	1.00
6e02f1e3	1.00	1.00	0.89	1.00	1.00	1.00	0.96